Adsorption (2014) 20:321–330
DOI 10.1007/s10450-013-9595-3

Adsorption of carbon dioxide on graphene oxide supported layered double oxides

Diana Iruretagoyena · Milo S. P. Shaffer · David Chadwick

Received: 18 May 2013 / Accepted: 24 November 2013 / Published online: 5 December 2013

Abstract Adsorption of CO_2 on layered double oxides supported on graphene oxide has been studied under dry and wet conditions. In the first exposure to the adsorptive gas, the isotherms obtained for supported and unsupported materials are shown to fit to the Freundlich model indicating the existence of heterogeneous adsorption sites. After multiple temperature-swing cycles, the adsorption capacity decreased and the data is better described by the Langmuir model. The presence of graphene oxide is shown to reduce the loss of adsorption capacity, and helps to maintain the heterogeneity of the basic sites on the adsorbents. The use of wet gas mixtures was found to have a positive effect on the CO_2 adsorption capacity of the graphene oxide hybrids. The presence of residual sodium on the materials resulted in a Freundlich isotherm with increased adsorption capacity.

Keywords Graphene oxide (GO) · Layered double hydroxide(s) (LDHs) · Hydrotalcite(s) · Layered double oxide(s) (LDOs) · CO_2 adsorption · Adsorption isotherms

List of symbols

b	Gas–solid interaction parameter in Langmuir isotherm (bar^{-1})
k	Pre-factor in Freundlich isotherm (mol kg_{ads}^{-1} $bar^{(-1/n)}$)
m	Monolayer capacity in Langmuir isotherm (mol kg_{ads}^{-1})
m_a	Mass of adsorbent within the column (kg)
n	Fitting parameter in Freundlich isotherm
P_b	Pressure inside the bed (bar)
P_s	Standard pressure (bar)
$P_{CO_{2f}}$	Partial pressure of CO_2 in the feed (bar)
q	Adsorption capacity (mol CO_2 kg_{ads}^{-1})
Q_{Ar-bk}	Volumetric flow rate of argon in the blank test (L min^{-1})
Q_f	Volumetric feed flow rate at standard conditions (L min^{-1})
t^o	Time to approach the effluent composition $y_{CO_{2f}}$ (min)
T_b	Temperature inside the bed (K)
T_s	Standard temperature (K)
t_{st}	Stoichiometric time of the column (min)
V_b	Volume of the bed (L)
y_{Ar}	Mol fraction of Ar at the exit of the column
y_{Arf}	Mol fraction of Ar in the feed
y_{CO_2}	Mol fraction of CO_2 at the exit of the column
$y_{CO_{2f}}$	Mol fraction of CO_2 in the feed
ε_T	Total porosity

D. Iruretagoyena · D. Chadwick (✉)
Department of Chemical Engineering, Imperial College London, South Kensington Campus, London SW7 2AZ, UK
e-mail: d.chadwick@imperial.ac.uk

M. S. P. Shaffer
Department of Chemistry, Imperial College London, South Kensington Campus, London SW7 2AZ, UK

1 Introduction

Hydrotalcite (HT) like compounds are receiving considerable attention due to their unique basic properties and to the increasing necessity to remove acidic molecules, e.g. H_2S, SO_x, HCl and CO_2, from many process and waste streams (Corma et al. 1994; Tong et al. 2011; Wang et al.

2011; Kang et al. 2013). In the context of CO_2 capture, hydrotalcites exhibit high CO_2 selectivity and fast adsorption kinetics even in the presence of competing species, being an outstanding adsorbent in the temperature range from 473 to 723 K. It has been reported that the CO_2 capacity and the multicycle stability of HT are enhanced in the presence of water, which makes these adsorbents suitable for wet applications (Ding and Alpay 2000; Jang et al. 2012). Similarly, hydrotalcites can be used to process sour gases containing carbon dioxide since the removal of CO_2 and H_2S can be carried out simultaneously (van Dijk et al. 2011).

Hydrotalcites, also known as layered-double hydroxides (LDHs), are two dimensional nanostructured materials composed of $M^{2+}(OH)_2$ layers in which divalent cations are partially substituted by trivalent cations. This creates a net positive charge that is compensated by anionic species and water molecules located in the space between the layers. The charge-neutral LDH structure can be expressed as $\left(M^{2+}_{1-x}M^{3+}_{x}(OH)_2\right)^{x+}\left(A^{m-}_{x/m}\cdot nH_2O\right)^{x-}$ where M^{2+}, M^{3+} and A^{m-} commonly represent Mg^{2+}, Al^{3+} and CO_3^{2-} respectively. These materials are significantly more active for the removal of carbon dioxide after thermal decomposition (above 400 °C), being transformed into nearly-amorphous layered double oxides (LDOs). Compared to other potential chemisorbents such as calcium oxides and lithium zirconates, LDOs show faster adsorption–desorption kinetics and the energy required in their regeneration is significantly lower (Choi et al. 2009). However, despite these positive properties, hydrotalcite derived materials show relatively low adsorption capacities and their long-term stability needs to be further improved for the successful implementation of temperature- and pressure-swing processes. Enhanced capacities can be obtained through the modification of the divalent to trivalent cation ratio, the substitution of the metal constituents, the addition of rare earths, and the promotion with alkali metals (e.g. Na, K, and Cs) (Yong et al. 2001; Hutson and Attwood 2008; Oliveira et al. 2008; Walspurger et al. 2008). On the other hand, the multicycle stability of LDOs can be improved by dispersing the particles over high surface area materials, which also leads to a moderate increment in the intrinsic adsorption capacity of the hydrotalcite derivatives (Meis et al. 2010a; Garcia-Gallastegui et al. 2012a).

Different supports for hydrotalcites have been reported including zeolites (Othman et al. 2006), carbon nanofibres (Meis et al. 2010a), alumina (Aschenbrenner et al. 2011) and multi-walled carbon nanotubes (Garcia-Gallastegui et al. 2012a). Although the resulting hybrids have shown better CO_2 adsorption performances compared to the pure HT, the improvement is observed only at very high dispersion, i.e. with low loadings of hydrotalcite over the support. This causes a severe decrease in the CO_2 capacity per volume of adsorbent which results in sorption units of impractical size. Recently we reported that by using small amounts of graphene oxide (GO) as support, the multicycle stability of LDOs is improved to a greater extent than with the other reported materials while an adequate capacity per volume of sorbent is maintained (Garcia-Gallastegui et al. 2012b). The effect was attributed to the formation of thinner platelets and to their dispersion in a charge-complementary 2D support that lead to an increase in effective hydrotalcite surface area.

The accurate description of the adsorption equilibrium is crucial for the prediction of the performance of large scale units. However, due to differences in the operating conditions, the composition, preparation mode and the use of promoters, there are some inconsistencies in the models used in the literature to describe the CO_2 adsorption isotherms of hydrotalcite derivatives. Langmuir isotherms have been extensively used although in some cases modifications have been made to account for chemical complexation or for the presence of two different adsorption sites (Ding and Alpay 2000; Lee et al. 2007; Oliveira et al. 2008). On the other hand, the Freundlich model has been applied mainly for low to intermediate CO_2 partial pressures (Soares et al. 2005; Reijers et al. 2009; Halabi et al. 2012). In this contribution we present an investigation of CO_2 adsorption over a range of CO_2 partial pressures by LDOs supported on GO as a novel sorbent. The experimental data for CO_2 adsorption obtained from TGA studies under dry conditions and from breakthrough analyses under both dry and wet conditions are fitted to Langmuir or Freundlich isotherms. The behaviour of the hybrid sorbent is compared with the unsupported hydrotalcite derivative. This extends the research on GO supported LDOs reported previously (Garcia-Gallastegui et al. 2012b) which focussed on the development of the sorbents and their stability. The effect of sodium as a promoter is also investigated in this work.

2 Experimental

2.1 Synthesis

Unsupported HT, $Mg_{0.6}Al_{0.3}(OH)_2(CO_3)_{0.15}\cdot nH_2O$, was synthesised by co-precipitation. To prepare 1 g of HT, an aqueous solution (4.5 ml) containing 9 mmol Mg $(NO_3)_2\cdot 6H_2O$ and 4.5 mmol $Al(NO_3)_3\cdot 9H_2O$ was added dropwise to an aqueous solution (6.7 ml) containing 8 mmol Na_2CO_3 and 32 mmol NaOH under vigorous stirring. The inorganic salts used in the synthesis were purchased from Sigma-Aldrich. The measured pH of the solution was 10. The resulting white suspension was aged

at 333 K for 12 h under vigorous stirring. Subsequently, the precipitate was filtered using 0.2 μm nylon membranes and thoroughly washed with DI water (0.5 L per 1 g of solid) at 333 K. Samples were dried for 12 h at 393 K in a recirculating oven.

In order to prepare HT/GO hybrids, GO (Nanoinnova Technologies) was dispersed in the alkali solution from which the HT was co-precipitated. The amount of GO added depended on the desired loading of GO in the hybrid. Two different HT/GO hybrids were prepared with weight nominal ratios 20/1 (HT_{20}) and 3/1(HT_3). The samples were filtered, washed and dried as described earlier for the unsupported HT. For comparison, a sample with an HT/GO ratio 20/1 was prepared and filtered with minimum washing to assess the effect of residual sodium ($HT_{20\text{-}Na}$). Typically 5 g of adsorbent were synthesised per batch.

2.2 Characterisation

N_2 physisorption measurements at 77 K were conducted using a Micrometrics Tristar 3000 instrument. The samples were dried at 393 K under N_2 for at least 12 h. The surface area was determined by the BET method and the pore volume was measured at P/Po = 0.991. The average pore diameter was calculated from the desorption isotherm using the BJH method. Powder X-ray diffraction (XRD) was carried out using a PAnalytical X'Pert Pro diffractometer (Cu Kα radiation) in reflection mode at room temperature. The elemental composition of the adsorbents was measured by Inductively Coupled Plasma-Optical Emission Spectroscopy (ICP-OES) in a Perkin Elmer Optima 2000DV apparatus. Thermo-gravimetric analysis (TGA), performed in a TAQ500 instrument, was used to determine the actual loading of GO in the hybrids. Approximately 5 mg of sample were dried at 393 K under N_2 for 20 min and then heated from 393 to 1,273 K at 10 K min^{-1} in 60 ml min^{-1} of air. Transmission electron microscopy (TEM) images were obtained using a JEOL 2000FX microscope and scanning electron microscopy (SEM) images were collected in a Zeiss Auriga FIB/FEG-SEM instrument.

2.3 CO_2 adsorption experiments

2.3.1 Thermogravimetric measurements

TGA was used to obtain adsorption isotherms under dry conditions. The samples were activated (calcined) in situ flowing 60 ml min^{-1} of N_2 at 673 K for 4 h to produce the corresponding unsupported LDO and the hybrids LDO_{20}, LDO_3 and $LDO_{20\text{-}Na}$. The adsorption isotherms were obtained using premixed gases: 2, 10, 15, 20, 50, 80, 99 % (v/v) CO_2 in Ar. Following the temperature treatment, CO_2 adsorption was carried out at 573 K for 30 min keeping the volumetric flow rate of the activation. In multicycle experiments a mixture 15 % CO_2/Ar was used during the adsorption cycle, and the desorption step was performed increasing the temperature to 673 K in flowing nitrogen (60 ml min^{-1}) for 30 min. After a near-constant capacity was obtained (typically ten cycles), the adsorption isotherm was measured continuing the adsorption–desorption cycles but increasing successively the concentration of CO_2 in the adsorption step using the premixed gases.

2.3.2 Breakthrough experiments and procedure

A stainless steel fixed bed column (ID = 6.9 mm, L = 364 mm) heated by a concentric furnace was used. The column was packed using 7 ml of silicon carbide (size 764 μm) followed by 1 g of sorbent material (250–500 μm). A stainless steel hollow rod with an orifice size of 1.6 mm was placed after the adsorbent bed to minimize the dead volume. The temperature was measured in the centre of the adsorbent bed using a type-K thermocouple. Two independent feeding lines, CO_2/Ar mixtures and nitrogen, were used to produce the desired step change by means of an electrically actuated four-way valve. The gas flow rates were regulated through two mass flow controllers. To conduct experiments in the presence of steam, the CO_2/Ar line was directed to an electrically heated vaporisation system to which water was fed using an HPLC or a syringe pump. All the lines of the system (stainless steel, 1.6 mm) were trace heated at 453 K to avoid condensation. A mass spectrometer (ESS GeneSys II) with heated capillary was used to monitor the effluent of the column. A water trap was placed before the sampling line.

For the breakthrough experiments 1 g of as-synthesised adsorbent was loaded in the column. The adsorbents were activated in situ under N_2 (138 ml min^{-1}) for 4 h at 673 K and the adsorption was conducted at 573 K. Typical flows of CO_2/Ar were 46 ml min^{-1} and for the wet experiments 9.3 ml min^{-1} of steam were usually added. The breakthrough was monitored for 30 min. All the isotherms were obtained from the adsorption capacity after the first exposure to the corresponding concentration of adsorptive gas using new material. Some multicycle tests with temperature swing and isothermal N_2 purge were also carried out. In the N_2 purge runs, desorption was conducted for 30 min under dry N_2 using the volumetric flow rate and temperature of the adsorption step. For the regeneration in temperature-swing cycles, the temperature was increased to 673 K passing N_2 during 30 min. All the experiments were carried out under an absolute pressure of 1 bar. During the activation step there is a weight loss of 40 % mainly due to dehydration, partial dehydroxylation and decarbonation of the HT component. At the end of the experiment the weight

of the recovered material was approximately 0.6 g. The moles of CO_2 adsorbed were calculated using the material balance in the column and assuming ideal gas behaviour (Lee et al. 2007) as in Eq. (1). The mass of adsorbent recovered was used (m_a) to normalise the CO_2 capacity.

$$q = \frac{Q_f P_s}{RT_s m_a}\left[t^o y_{CO_{2f}} - y_{Arf}\int_0^{t^0}\frac{y_{CO_2}}{y_{Ar}}dt\right] - \frac{\varepsilon_T V_b P_b y_{CO_{2f}}}{RT_b m_a} \quad (1)$$

The dead-volume of the adsorption unit ($\varepsilon_T V_b$) was obtained from a blank experiment using the packed column and switching from nitrogen to argon, where

$$\varepsilon_T V_b = t_{st} Q_{Ar-bk} \quad (2)$$

2.3.3 Fitting of the adsorption isotherms

The adsorption capacity of the materials was taken as the average of at least three measurements under the same operating conditions. The individual values were used to calculate the corresponding standard deviations in the mean. For the adsorption isotherms of the materials after multiple cycles, the standard deviation in the mean was calculated from the adsorption capacity after ten cycles obtained in at least three different experiments (see 2.3.1 and 2.3.2). This error was assumed to be the same for the adsorption capacities obtained at the different CO_2 partial pressures. The experimental adsorption isotherms were fitted to Langmuir (3) and Freundlich (4) models applying a nonlinear least square method using OriginPro8.6.

$$q = \frac{mbP_{CO_2}}{1 + bP_{CO_2}} \quad (3)$$

$$q = k[P_{CO_2}]^{1/n} \quad (4)$$

Direct fitting of adsorption data using nonlinear regression is usually preferred as it avoids the problems of changing error distribution and biased parameters associated with linear transformations (Kinniburgh 1986).

3 Results and discussion

3.1 Characterisation of the adsorbents

The composition and the physicochemical properties of the materials are presented in Table 1. The actual Mg/Al ratios measured by ICP are consistent with the nominal values for the unsupported and supported materials. Sodium was detected only at trace levels for the thoroughly washed hybrids, while 2 % of sodium was measured for the minimum washed sample ($HT_{20\text{-}Na}$). The loading of GO was determined experimentally by thermogravimetric analysis considering the residues of the pure materials at 973 K. Details of this technique are available elsewhere (Garcia-Gallastegui et al. 2012b). The nominal and actual weight loadings are very close for the samples with an HT/GO ratio 20:1 but for the ratio 3:1 the amount of GO is lower than expected. This is in agreement with previous findings showing that the loss of oxidative debris during filtering becomes more significant as the GO content in the sample increases (Rourke et al. 2011; Garcia-Gallastegui et al. 2012b).

The BET surface areas of the as-synthesised and calcined unsupported and supported hydrotalcites are high compared to other reported values for similar synthesis methods (Meis et al. 2010a; Garcia-Gallastegui et al. 2012b). This is assumed to be caused by an improved control of the stirring and the addition rate of the solution containing the Mg and Al nitrates. As a consequence of the higher surface areas obtained, the loadings of GO required to observe an enhancement in the dispersion of the as-synthesised hybrids are slightly higher than those reported previously by Garcia-Gallastegui et al. (2012b). The surface areas of LDO_{20} and LDO_3 are smaller than that of the pure LDO. GO restacking becomes more significant as the content of LDO is reduced in the hybrid resulting in lower surface areas (Garcia-Gallastegui et al. 2012b).

The XRD patterns of the as-synthesised materials and the support are presented in Fig. 1. The GO reflections are consistent with previous reports (Garcia-Gallastegui et al. 2012b). The HT-containing samples display the characteristic reflections corresponding to bi-dimensional hydrotalcite-like materials (JCPDS No. 14-191) and can be indexed accordingly (Millange et al. 2000). No diffraction peaks associated with GO were observed for the hybrids, which is in agreement with SEM and TEM results where GO flakes were not detected. It is assumed that for these loadings, the GO nanosheets are well integrated with the HT particles improving their dispersion. Therefore, the diffraction peaks of HT become broader with increasing amount of support resulting in smaller crystallites. For the minimum washed sample $HT_{20\text{-}Na}$, a diffraction line representative of $NaNO_3$ (104) is observed (Leon et al. 2010). The presence of residual sodium in the sample results in a small decrease in the BET surface areas and pore volumes of the as-synthesised and calcined samples given in Table 1. The corresponding LDO samples show broad peak reflections ascribed to the diffraction planes of periclase (MgO, JCPDS No. 45-946); the aluminium is thought to be well dispersed (Leon et al. 2010). $NaNO_3$ is decomposed during the thermal treatment releasing NO_x and sodium remains on the surface of the solid. The calcination of GO led to XRD patterns with graphitic (002) and (100) lattice planes (Fig. 2).

Table 1 Physicochemical properties of the adsorbents

As-synthesised adsorbents								Activated adsorbents			
Sample name[a]	wt% GO Nom.	wt% GO Actual	Mg/Al (mol/mol)	wt% Na	Crystallite size (003) (nm)	S_{BET} (m^2/g)	Pore volume (cm^3/g)	Sample name[a]	S_{BET} (m^2/g)	Pore volume (cm^3/g)	$molCO_2/kg^b_{ads}$
Pure HT	0	0	2.20	0.03	21	112	0.46	Pure LDO	223	0.51	0.27 ± 0.01
HT_{20}	5	4	2.19	0.10	20	106	0.54	LDO_{20}	199	0.62	0.27 ± 0.02
HT_3	25	16	2.22	0.20	11	143	0.47	LDO_3	170	0.54	0.25 ± 0.01
$HT_{20\text{-}Na}$	5	6	2.22	1.90	24	70	0.38	$LDO_{20\text{-}Na}$	116	0.48	0.54
GO	100	100	–	–	–	55	0.06	GO	81	0.15	Negligible

[a] HT_x and LDO_x where x is the nominal HT to GO weight ratio of the precalcined sample

[b] First-contact adsorption capacity (shown with standard errors) measured at 573 K and $PCO_2 = 0.15$ bar

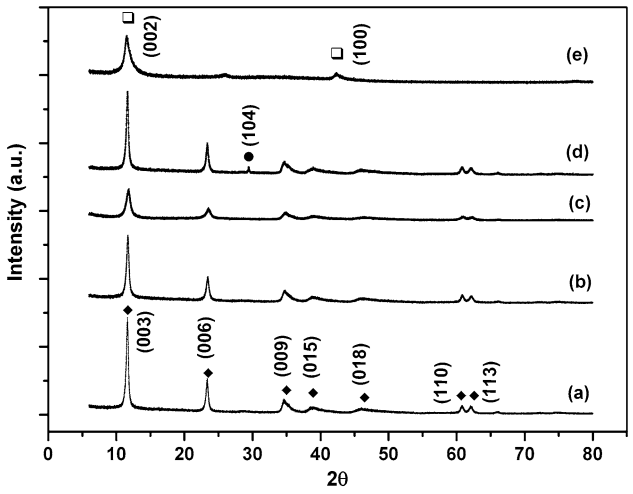

Fig. 1 XRD diffraction patterns of *a* Pure HT, *b* HT_{20}, *c* HT_3, *d* $HT_{20\text{-}Na}$ and *e* GO. Characteristic reflections of HT (*diamond*), $NaNO_3$ (*dot*) and GO (*square*)

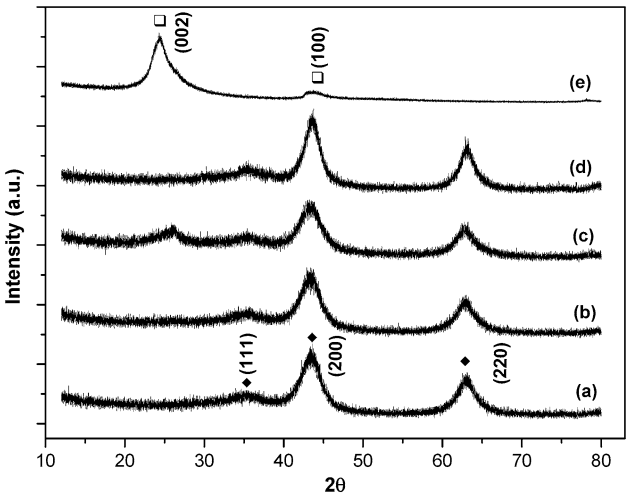

Fig. 2 XRD diffraction patterns of *a* pure LDO, *b* LDO_{20}, *c* LDO_3, *d* $LDO_{20\text{-}Na}$, and *e* calcined GO (×0.2). Characteristic reflections of calcined HT (*diamond*) and calcined GO (*square*)

3.2 Dry adsorption isotherms

The CO_2 capacities were measured by thermogravimetric and breakthrough curve analyses which showed good agreement, validating the methodology used. The experimental results of the adsorption isotherms obtained by TGA at 573 K for the pure LDO and LDO_{20} were fitted to the Langmuir and Freundlich models. The experimental data and the fittings for the first-contact-adsorption (equilibrium capacity in the first exposure to the adsorptive gas after activation), and after continuous temperature-swing cycles carried out in the TGA are presented in Figs. 3 and 4. The associated derived parameters are given in Table 2.

First-contact-adsorption by the pure LDO and LDO_{20} is better described by the Freundlich rather than the Langmuir isotherm, although the difference is only just statistically significant for the range of conditions studied. The values

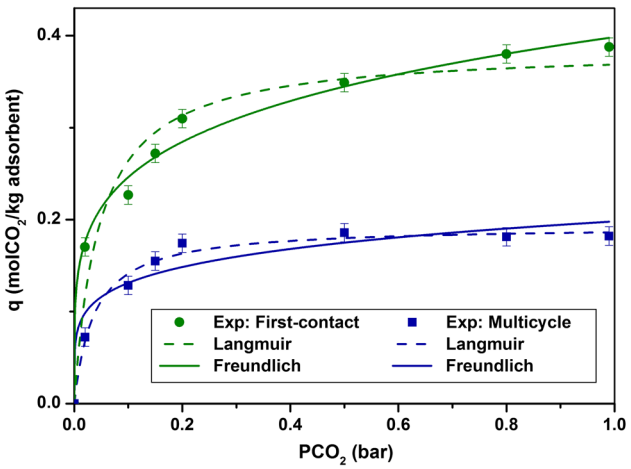

Fig. 3 First-contact and multicycle adsorption isotherms at 573 K under dry conditions from TGA measurements for pure LDO; shown with standard errors

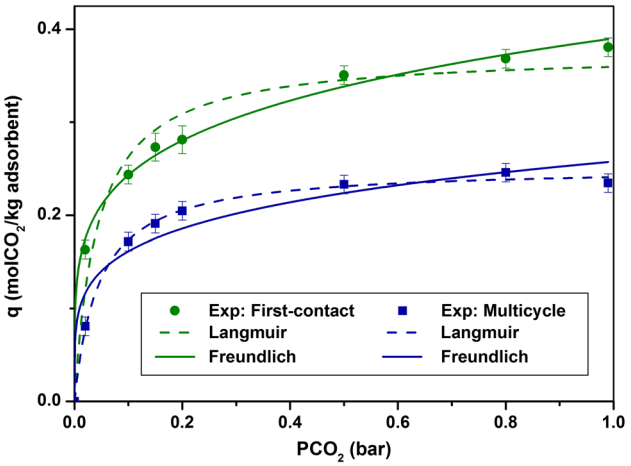

Fig. 4 First-contact and multicycle adsorption isotherms at 573 K under dry conditions from TGA measurements for LDO_{20}; shown with standard errors

of the Freundlich gas–solid interaction parameter, *k*, are similar for both materials indicating that the presence of GO does not modify significantly the nature of the adsorption sites. The residual adsorption capacity after ten adsorption–desorption cycles for the pure LDO is 58 % compared to 70 % for LDO_{20}, in agreement with the improvement in the stability previously reported by Garcia-Gallastegui et al. (2012b).

The isotherms of LDO and LDO_{20} obtained after multiple cycles are also shown in Figs. 3 and 4. These were found to fit better to the Langmuir model, indicating that upon adsorption–desorption temperature cycling the heterogeneity of the adsorption sites tends to disappear rendering a more ideal uniform surface.

The stability of the adsorption capacity was also explored in both N_2 purge and temperature-swing breakthrough experiments using the hybrid LDO_{20} (Fig. 5a, b respectively). In both cases, there is a significant loss of capacity during the first-contact-adsorption which is caused by the irreversible chemisorption of CO_2 over the strongest basic sites created during the activation. In the N_2 purge almost all the loss in capacity is in the first contact. The capacity recovered in the first temperature-swing cycle is higher than in the first N_2 purge cycle due to the thermal activation of the desorption process. From the second temperature-swing cycle, there is a progressive small decrease in the adsorption capacity, which may be due to the gradual evolution of the LDO particles in a process that is likely to be temperature-driven. After the first cycle in N_2 purge experiments, the adsorption capacity is more stable and mainly weak-chemisorption sites are cyclically occupied and evacuated. Other authors have reached the same conclusion from the values of the heat of adsorption calculated between 673 and 793 K (Ding and Alpay 2000; Lee et al. 2007, Leon et al. 2010).

The adsorption isotherm and the parameters fitted for LDO_3 after being exposed to ten sorption cycles conducted in the TGA are presented in Fig. 6 and Table 2 respectively. The residual capacity for this hybrid was 83 %, which is a considerable improvement in the stability compared to the pure LDO and LDO_{20}. Additionally, the initial heterogeneity of LDO_3 appears to be maintained after the temperature-swing experiments, as revealed from the better fit of the equilibrium data to the Freundlich model. Consideration of the values in Table 1 suggests that the *intrinsic* first-contact adsorption capacities (i.e. normalised per mass of LDO) are close for the unsupported LDO and the hybrids, revealing that the nature and number of basic sites are initially similar. Adsorption of CO_2 on layered double oxides takes place over basic oxygen sites, the strength of which depends on their coordination as discussed by Meis et al. (2010a). We speculate that GO helps to prevent the degradation of the LDO crystallites and an associated decrease in the number of defects, i.e. oxygen atoms located at the edges and corners, maintaining the heterogeneity of the adsorption sites. Since the defects have stronger basicity than the atoms in the basal planes, the CO_2 capacity (*intrinsic* and total, i.e. per kg of total adsorbent) is better preserved after multiple cycles in the LDO/GO hybrids. However, it is possible that after further extensive cycling LDO_3 would eventually become better described by the Langmuir isotherm.

Table 2 Parameters for adsorption isotherms at 573 K from TGA under dry conditions

Adsorbent	Langmuir isotherm[a]		Freundlich isotherm[a]	
	m (mol/kg)	b (1/bar)	k (mol/kg)	*n* (-)
Pure LDO (first-contact)	0.39 ± 0.02	21.7 ± 6.5	0.40 ± 0.01	4.78 ± 0.38
Pure LDO (multicycle)	0.19 ± 0.01	27.2 ± 4.3	0.20 ± 0.01	5.58 ± 1.28
LDO_{20} (first-contact)	0.37 ± 0.02	23.5 ± 6.3	0.39 ± 0.01	4.86 ± 0.25
LDO_{20} (multicycle)	0.25 ± 0.00	22.2 ± 1.5	0.26 ± 0.01	4.91 ± 0.91
LDO_3 (multicycle)	0.30 ± 0.01	18.1 ± 3.9	0.31 ± 0.01	4.35 ± 0.33

[a] The parameters are shown with the standard errors obtained from the fittings

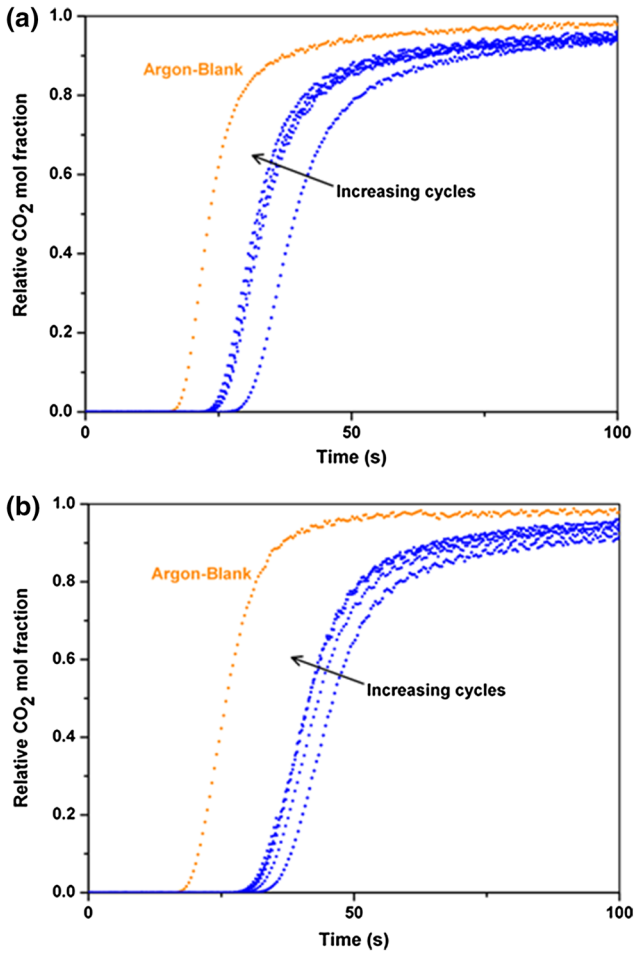

Fig. 5 **a** N_2 purge (six cycles; adsorption 573 K; desorption 573 K) and **b** temperature-swing (six cycles; adsorption 573 K; desorption 673 K). Adsorbent: LDO_{20}; $P_{CO_2f} = 0.1$ bar; dry conditions

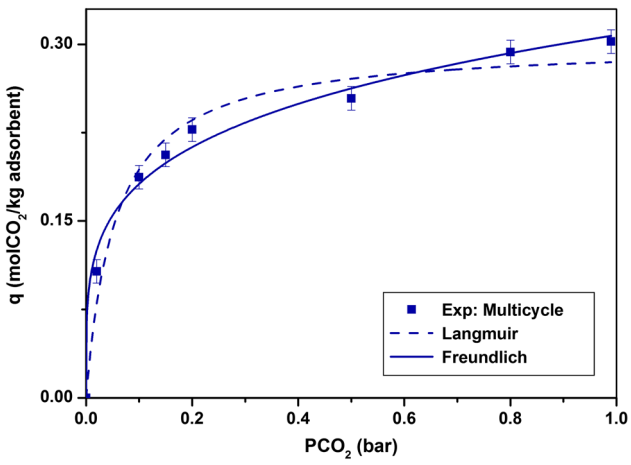

Fig. 6 Multicycle adsorption isotherm at 573 K under dry conditions from TGA measurements for LDO_3; shown with standard errors

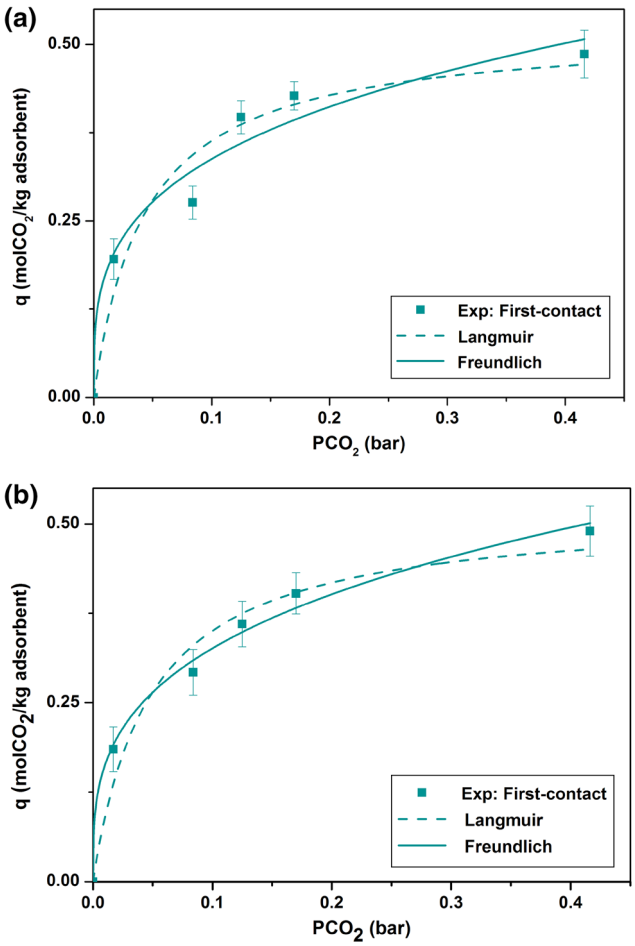

Fig. 7 First-contact adsorption isotherms at 573 K under wet conditions obtained from breakthrough analysis for **a** pure LDO and **b** LDO_{20}; data shown with standard errors

3.3 Wet adsorption isotherms

The first-contact-adsorption isotherms under wet conditions (0.16 mol steam/mol total) for pure LDO and LDO_{20} were obtained from breakthrough analysis and are presented in Fig. 7a, b. Under the operating conditions, no sign of gasification of GO was observed. The presence of water has a beneficial effect on the adsorption properties of both materials, causing an increase in the CO_2 capacity. The adsorption of H_2O and CO_2 was observed to produce an increase in the temperature inside the column ($\Delta T = 21$ K) that is considerably higher than under dry conditions ($\Delta T = 4$ K). This result suggests that the exothermic surface rehydration leads to the creation of new sites for CO_2 adsorption, possibly aluminium and magnesium hydroxides as proposed by Ram Reddy et al. (2008). Temperature-swing multicycle experiments carrying out the adsorption in the presence of steam and the regeneration under dry nitrogen showed a loss of capacity similar to that obtained in completely dry cycles (data not show).

Table 3 Parameters for adsorption isotherms at 573 K under wet conditions from breakthrough analysis

Adsorbent	Langmuir isotherm[a]		Freundlich isotherm[a]	
	m (mol/kg)	b (1/bar)	k (mol/kg)	*n* (-)
Pure LDO (first-contact)	0.52 ± 0.05	23.1 ± 9.6	0.65 ± 0.06	3.50 ± 0.63
LDO_{20} (first-contact)	0.52 ± 0.05	20.9 ± 7.0	0.65 ± 0.03	3.31 ± 0.26

[a] The parameters are shown with the standard errors obtained from the fittings

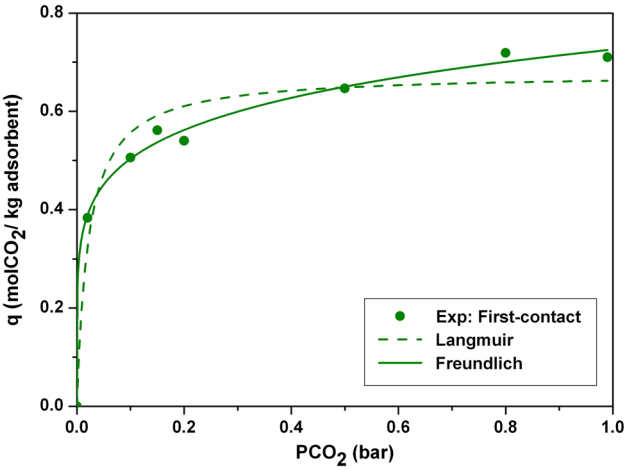

Fig. 8 First-contact adsorption isotherm at 573 K under dry conditions for $LDO_{20\text{-}Na}$

However, it has been reported that when adsorption and desorption are conducted in the presence of steam, the decrease in the adsorption capacity is more gradual since the formation of irreversible carbonates is prevented by the competing adsorption of water (Ding and Alpay 2000).

The wet adsorption data were fitted to the Langmuir and Freundlich models using Eqs. 3 and 4 (Fig. 7). The parameters are given in Table 3. These are only approximations to the real isotherms since the competitive adsorption of species should be considered and the column is not completely isothermal. In any case, the Freundlich isotherm was found to describe slightly better the equilibrium data for both adsorbents, although a clear distinction is difficult due to the magnitude of the error bars. To clarify the type of adsorption, experiments need to be conducted in a wider range of CO_2 partial pressure using more adsorbent.

3.4 Effect of residual sodium over the LDO/GO hybrid

The presence of residual sodium (2 wt%) was found to increase significantly the CO_2 adsorption capacity of the hybrid $LDO_{20\text{-}Na}$ (Fig. 8). The promoting effect of alkali metals (Na, K mainly) on LDOs has been widely reported and different explanations can be found in the literature. Based on DRIFTS studies and on the fact that potassium increases the CO_2 adsorption capacity of Al_2O_3 but was observed to have a very small effect on MgO, Walspurger et al. (2008) proposed that the interaction between aluminium oxide centres and potassium carbonate is crucial in the creation of strongly basic sites. In contrast, Meis et al. (2010b) proposed that alkali ions (Na^+, K^+) substitute Mg^{2+} on the surface of LDO and suggested that the oxygen atoms in the vicinity of the monovalent ions adsorb CO_2 more strongly. Our experimental data show that, as in the case of LDO_{20}, the first-contact adsorption over the hybrid $LDO_{20\text{-}Na}$ is better described by the Freundlich isotherm. This indicates that the relatively low content of sodium in the sample does not alter significantly the heterogeneity of the surface. The increment in the value of the gas–solid interaction parameters (Table 4) compared to the unpromoted hybrid (Table 2) reveals an increase in the basic strength of the adsorption sites with sodium. The adsorption parameters obtained are not directly comparable with previous reported work due to differences in the alkali promoter and the operating conditions used. However, it can be seen in Table 4 that the values obtained are in the same order of magnitude to those reported by Halabi et al. (2012). In addition, although a better agreement was found using the Freundlich equation (Fig. 8), the monolayer capacity and the interaction parameter obtained using the Langmuir model are comparable with data sets previously reported for potassium promoted hydrotalcites (Table 4).

4 Conclusions

The CO_2 adsorption capacity of the unsupported and GO-supported LDOs in the first exposure to the adsorptive gas are similar, indicating that GO does not modify significantly the nature of the adsorption sites. The first-contact adsorption data for the pure LDO and the GO hybrids is better described by the Freundlich isotherm but after multiple temperature-swing cycles the isotherms tend to fit to the Langmuir model as the surface becomes more uniform. Multicycle temperature swing and isothermal N_2 purge experiments suggested that the loss of CO_2 capacity after the first cycle is caused by irreversible adsorption over very strong basic sites that are created during the thermal activation. The adsorption capacity of the materials used in temperature-swing cycles decays more gradually, possibly indicating some additional thermal degradation. The use of GO as a support significantly enhances the thermal stability of the LDOs helping to maintain the number and

Table 4 Parameters for adsorption isotherms from alkali promoted LDO at 573 K under dry conditions

Authors	Adsorbent	Langmuir isotherm[a]		Freundlich isotherm[a]	
		m (mol/kg)	b (1/bar)	k (mol/kg)	*n* (-)
Present work (first-contact)	$LDO_{20\text{-}Na}$	0.68 ± 0.03	46.3 ± 15.3	0.73 ± 0.01	6.28 ± 0.39
Hufton et al. (1999)	K promoted LDO	0.45	94.6[b]	–	–
Ding and Alpay (2000)	K promoted LDO	0.63	23.1[b]	–	–
Lee et al. (2007)	K promoted LDO	0.25	73.3[b]	–	–
Halabi et al. (2012)	K promoted LDO	–	–	1.04[c]	1.68[c]

[a] The parameters are shown with the standard errors obtained from the fittings

[b] The values of b at 573 K were obtained using the heats of adsorption reported in the references

[c] Parameters reported at 673 K

heterogeneity of the adsorption sites for a longer number of temperature-swing cycles. Water was shown to have a positive effect on the adsorption capacity of unsupported LDO and a GO hybrid. Under the conditions of the experiments, there was no evidence of graphene gasification. Residual sodium over GO-supported LDO promotes the basic strength of the adsorption sites which enhances significantly the CO_2 adsorption capacity while favouring the Freundlich isotherm.

Acknowledgments The authors are grateful to Ainara Garcia-Gallastegui and Raul Montesano for discussions and assistance. D.I. thanks CONACyT and SEP for the scholarships awarded.

References

Aschenbrenner, O., McGuire, P., Alsamaq, S., Wang, J., Supasitmongkol, S., Al-Duri, B., Styring, P., Wood, J.: Adsorption of carbon dioxide on hydrotalcite-like compounds of different compositions. Chem. Eng. Res. Des. **89**, 1711–1721 (2011)

Choi, S., Drese, J.H., Jones, C.W.: Adsorbent materials for carbon dioxide capture from large anthropogenic point sources. ChemSusChem. **2**, 796–854 (2009)

Corma, A., Palomares, A.E., Rey, F.: Optimization of SO_X additives of FCC catalysts based on MgO–$A1_2O_3$ mixed oxides produced from hydrotalcites. Appl. Catal. B **4**, 29–43 (1994)

Ding, Y., Alpay, E.: Equilibria and kinetics of CO_2 adsorption on hydrotalcite adsorbent. Chem. Eng. Sci. **55**, 3461–3474 (2000)

Garcia-Gallastegui, A., Iruretagoyena, D., Mokhtar, M., Asiri, A.M., Basahel, S.N., Al-Thabaiti, S.A., Alyoubi, A.O., Chadwick, D., Shaffer, M.S.P.: Layered double hydroxides supported on multiwalled carbon nanotubes: preparation and CO_2 adsorption characteristics. J. Mater. Chem. **22**, 13932–13940 (2012a)

Garcia-Gallastegui, A., Iruretagoyena, D., Gouvea, V., Mokhtar, M., Asiri, A.M., Basahel, S.N., Al-Thabaiti, S.A., Alyoubi, A.O., Chadwick, D., Shaffer, M.S.P.: Graphene oxide as support for layered double hydroxides: enhancing the CO_2 adsorption capacity. Chem. Mater. **24**, 4531–4539 (2012b)

Halabi, M.H., de Croon, M.H.J.M., van der Schaaf, J., Cobden, P.D., Schouten, J.C.: High capacity potassium-promoted hydrotalcite for CO_2 capture in H_2 production. Int. J. Hydrogen Energy **37**, 4516–4525 (2012)

Hufton, J.R., Mayorga, S., Sircar, S.: Sorption-enhanced reaction process for hydrogen production. AIChE J. **45**, 248–256 (1999)

Hutson, N.D., Attwood, B.C.: High temperature adsorption of CO_2 on various hydrotalcite-like compounds. Adsorption **14**, 781–789 (2008)

Jang, H.M., Lee, K.B., Caram, H.S., Sircar, S.: High-purity hydrogen production through sorption enhanced water gas shift reaction using K_2CO_3-promoted hydrotalcite. Chem. Eng. Sci. **73**, 431–438 (2012)

Kang, H.T., Lv, K., Yuan, S.L.: Synthesis, characterization, and SO_2 removal capacity of MnMgAlFe mixed oxides derived from hydrotalcite-like compounds. Appl. Clay Sci. **72**, 184–190 (2013)

Kinniburgh, D.G.: General purpose adsorption isotherms. Environ. Sci. Technol. **20**, 895–904 (1986)

Lee, K.B., Verdooren, A., Caram, H.S., Sircar, S.: Chemisorption of carbon dioxide on potassium-carbonate-promoted hydrotalcite. J. Colloid Interface Sci. **308**, 30–39 (2007)

Leon, M., Diaz, E., Bennici, S., Vega, A., Ordonez, S., Auroux, A.: Adsorption of CO_2 on hydrotalcite-derived mixed oxides: sorption mechanisms and consequences for adsorption irreversibility. Ind. Eng. Chem. Res. **49**, 3663–3671 (2010)

Meis, N.N.A.H., Bitter, J.H., de Jong, K.P.: Support and size effects of activated hydrotalcites for precombustion CO2 capture. Ind. Eng. Chem. Res. **49**, 1229–1235 (2010a)

Meis, N.N.A.H., Bitter, J.H., de Jong, K.P.: On the influence and role of alkali metals on supported and unsupported activated hydrotalcites for CO_2 sorption. Ind. Eng. Chem. Res. **49**, 8086–8093 (2010b)

Millange, F., Walton, R.I., O'Hare, D.: Time-resolved in situ X-ray diffraction study of the liquid-phase reconstruction of Mg–Al-carbonate hydrotalcite-like compounds. J. Mater. Chem. **10**, 1713–1720 (2000)

Oliveira, E.L.G., Grande, C.A., Rodrigues, A.E.: CO_2 sorption on hydrotalcite and alkali-modified (K and Cs) hydrotalcites at high temperatures. Sep. Purif. Technol. **62**, 137–147 (2008)

Othman, M.R., Rasid, N.M., Fernando, W.J.N.: Mg–Al hydrotalcite coating on zeolites for improved carbon dioxide adsorption. Chem. Eng. Sci. **61**, 1555–1560 (2006)

Ram Reddy, M.K., Xu, Z.P., Lu, G.Q., Diniz da Costa, J.C.: Influence of water on high-temperature CO_2 capture using layered double hydroxide derivatives. Ind. Eng. Chem. Res. **47**, 2630–2635 (2008)

Reijers, H.T.J., Boon, J., Elzinga, G.D., Cobden, P.D., Haije, W.G., van den Brink, R.W.: Modeling study of the sorption-enhanced reaction process for CO_2 capture. I. Model development and validation. Ind. Eng. Chem. Res. **48**, 6966–6974 (2009)

Rourke, J.P., Pandey, P.A., Moore, J.J., Bates, M., Kinloch, I.A., Young, R.J., Wilson, N.R.: The real graphene oxide revealed: stripping the oxidative debris from the graphene-like sheets. Angew. Chem. Int. Ed. **50**, 3173–3177 (2011)

Soares, J.L., Casarin, G.L., Jose, H.J., Moreira, R.D.F.P.M.: Experimental and theoretical analysis for the CO_2 adsorption on hydrotalcite. Adsorption **11**, 237–241 (2005)

Tong, M., Chen, H., Yang, Z., Wen, R.: The effect of Zn–Al-hydrotalcites composited with calcium stearate and β-diketone on the thermal stability of PVC. Int. J. Mol. Sci. **12**, 1756–1766 (2011)

van Dijk, H.A.J., Walspurger, S., Cobden, P.D., van den Brink, R.W., de Vos, F.G.: Testing of hydrotalcite-based sorbents for CO_2 and H_2S capture for use in sorption enhanced water gas shift. Int. J. Greenhouse Gas Control **5**, 505–511 (2011)

Walspurger, S., Boels, L., Cobden, P.D., Elzinga, G.D., Haije, W.G., van den Brink, R.W.: The crucial role of the K^+ -aluminium oxide interaction in K^+ -promoted alumina- and hydrotalcite-based materials for CO_2 sorption at high temperatures. ChemSusChem. **1**, 643–650 (2008)

Wang, Q., Luo, J., Zhong, Z., Borgna, A.: CO_2 capture by solid adsorbents and their applications: current status and new trends. Energy Environ. Sci. **4**, 42–55 (2011)

Yong, Z., Mata, V., Rodrigues, A.E.: Adsorption of carbon dioxide onto hydrotalcite-like compounds(HTlcs) at high temperatures. Ind. Eng. Chem. Res. **40**, 204–209 (2001)